Research Article Vol. 4, No. 7 / July 2017 / Optica 757

Probing the fundamental detection limit of photonic crystal cavities

Kumar Saurav[1,2] and Nicolas Le Thomas[1,2,*]

[1]Photonics Research Group, INTEC Department-Ghent University-imec, Gent, Belgium
[2]Center for Nano- and Biophotonics, Ghent University, 9000 Gent, Belgium
*Corresponding author: Nicolas. LeThomas@UGent.be

Received 3 April 2017; revised 30 May 2017; accepted 2 June 2017 (Doc. ID 292082); published 5 July 2017

The accurate characterization of single nanoparticles in colloidal solutions in terms of their size and morphology is important for medical diagnostics and aerosol investigations. However, it is challenging to achieve a high throughput for very small (sub-100 nm) particles. In particular, it is not well established what the fundamental limits are on the trade-off between speed and the smallest detectable particle. Here we study these limits for the case of refractive index sensing based on resonant photonic crystal cavities. Importantly, we have reached a regime where the fundamental thermal fluctuations set the intrinsic detection limit for acquisition sampling times t_{acq} larger than 3 μs. Such an intrinsic fundamental limit corresponds to 1/2000th the linewidth of the optical spectrum of photonic crystal cavities of effective mode volume as small as 0.06 μm^3. The results of this work indicate that it is possible to monitor up to 33 million particles per second with a particle size down to 34 nm, making it a promising technique for fast real-time biosensing.

OCIS codes: (130.0130) Integrated optics; (230.5298) Photonic crystals; (260.5740) Resonance; (270.2500) Fluctuations, relaxations, and noise; (280.4788) Optical sensing and sensors.

https://doi.org/10.1364/OPTICA.4.000757

1. INTRODUCTION

Optical microcavities, such as microspheres, microtoroids, microring resonators, or photonic crystal (PhC) cavities [1,2] have enabled the noninvasive detection of biological molecules, reaching even the single molecule level for sensing based on high-quality factor (Q factor) whispering gallery (WG) modes [3]. Reaching sensitivities at the level of a single nanoparticle is now sparking the challenge of accurately tracking its motion at an acquisition time in line with its inertial time, in view of sensing fast chemical or biological events at the nanoscale [4,5].

Increasing the acquisition speed unfortunately jeopardizes the amount of collected information, and consequently the detection limit. In this context, integrated PhC cavities can play a key role, as they feature both high Q factor and small mode volume [6], and their specific design enables an efficient signal collection. Nevertheless, their intrinsic detection limit versus the acquisition speed of the sensing signal has not been experimentally unveiled up to now.

Here, we experimentally investigate and accurately quantify the trade-off between the acquisition time and the detection limit of integrated silicon PhC cavities. As a result, a frequency-shift noise level amounting to 1/2000th the linewidth of the cavity mode has been achieved for an acquisition time and a mode volume as small as 3 μs and 0.06 μm^3, respectively. Such a noise floor originates from the fundamental thermal fluctuations of the medium and sets the ultimate detection limit of dielectric optical cavities.

The principle of optical cavity sensors relies on detecting shifts of the resonant frequency ω_0 of the cavity. The frequency shifts are induced by local perturbations of the refractive index map due to the presence of the nanoparticle under investigation. Knowing the optical spectrum of the cavity mode, one fast approach to quantify any spectral shifts consists of recording the fluctuations of the intensity I^{scat} of a single frequency laser field scattered by the cavity. In this case, the refractive index perturbation triggers a dynamic detuning between the fixed laser field frequency ω_p and the resonant frequency ω_0, which results in intensity fluctuations of the scattered field. As a forerunner experiment towards single nanoparticle tracking, the temporal variations of the local density of nanoparticle solutions near a WG mode were monitored with a 5 μs acquisition time by Keng *et al.* [7] for sizing purposes.

Using a high-quality-factor WG mode to retrieve reliable quantitative information about the fast Brownian motion of a single colloidal nanoparticle only from induced intensity fluctuations is difficult due to the presence of splitting and broadening of the mode spectrum that add to the expected frequency shift. In addition, implementing high-Q cavities requires a careful stabilization of the exciting laser source. To overcome these issues, we focus here on nondegenerate PhC cavity modes of sufficiently low Q factor and small mode volume V_{eff} [8], such as the fundamental mode of the L3 cavity presented in Fig. 1.

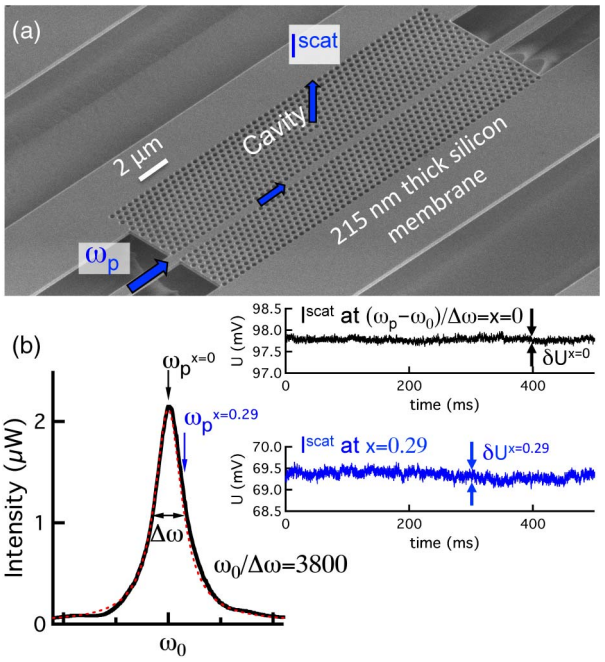

Fig. 1. (a) Scanning electron micrograph of the top surface of an integrated L3 PhC cavity. The silicon oxide has been removed below the 220 nm thick free-standing slab. The blue arrows indicate the light path of the pump laser beam at a frequency ω_p. (b) Experimental optical spectrum of the cavity (dark curve) with the corresponding Lorentzian fit (red dotted curve) whose cavity linewidth is $\Delta\omega = \omega_0/3800$. The resonant frequency ω_0 corresponds to a wavelength of 1599.3 nm. On the right: Time traces of the photovoltage induced by the collected scattered light I^{scat} for a $x = 0$ (black trace) and $x = 0.29$ (blue trace) frequency detuning. Each of the traces is made of 50,000 equidistant data points.

2. EXPERIMENT

A standard L3 PhC cavity is defined by removing three adjacent holes from a triangular lattice in the ΓK direction, i.e., in the direction of the in-plane blue arrows in Fig. 1(a). A W1 PhC waveguide, created by removing one line of holes also in the ΓK direction and separated by four lines of holes from the L3 defect, ensures the excitation of the fundamental resonant cavity mode. The light intensity I^{scat} that is scattered out-of-plane by the cavity is collected through a high-numerical-aperture (NA = 0.95) microscope objective and detected with a fast photodiode. A fast oscilloscope records the photo voltage U generated by the photodiode (see Section 7). By analyzing the noise on U, our purpose is to experimentally identify the main constraints on the acquisition speed and the minimal frequency shift that is detectable with a PhC cavity of a given Q factor and mode volume. The quality factor Q is defined as the ratio between the resonant frequency ω_0 and the linewidth $\Delta\omega$ of the optical spectrum of the cavity coupled to the access W1 waveguide.

As revealed by the black and blue temporal traces in Fig. 1(b), the photovoltage U induced by the scattered intensity I^{scat} at a load resistance $R_{load} = 11.8$ kΩ is subject to temporal fluctuations even without any intentional extrinsic perturbations of the PhC cavity. The origin of the observed noise is of diverse nature, as recently theoretically investigated in [9,10]. The most relevant noise contributions are the thermal noise in the load resistance (Johnson noise), the shot noise, the relative intensity noise (RIN) of the laser source, the frequency noise of the laser source, the thermorefractive noise resulting from the fundamental thermal fluctuations, and the noise contribution resulting from any mechanical vibrations. Some of these contributions are not intrinsic to the cavity, such as the noise contributions related to the laser pump, the photodetector, and the mechanical vibrations (see Section 7).

Importantly, the standard deviation δU of these fluctuations that is reported in Fig. 1(b) depends on the detuning between the frequencies of the pump and of the cavity resonance, $x = (\omega_p - \omega_0)/\Delta\omega = \delta\omega_p/\Delta\omega$. For zero detuning $x = 0$, the noise is 3 times lower than in the case of a blue-shifted detuning $x = 0.29$, which is the optimal value for sensing intensity variations induced by a cavity frequency shift. It implies that the intensity noises related to the laser source, the photodetection, and mechanical environment are not the main contributions at $x = 0.29$. The dependence of the noise on the detuning x is in line with a frequency noise, either on ω_0 or on ω_p.

To highlight the impact of the different contributions to the noise level, we have measured the scattered intensity I^{scat} for different load resistances. Lowering the load resistance decreases the possible acquisition sampling time t_{acq} at the expense of a lower signal voltage U. We define here the acquisition sampling time t_{acq} as the minimal response time that is needed to reach 99% of the average value of a steady state under a step variation of the signal. For a load resistance of 1 MΩ, $t_{acq} = 0.7$ ms, whereas for 560 Ω, the acquisition sampling time drops to 0.7 μs [11].

In Fig. 2, the noise-to-signal ratio of the photo voltage, defined as the ratio of the standard deviation δU to the average voltage U,

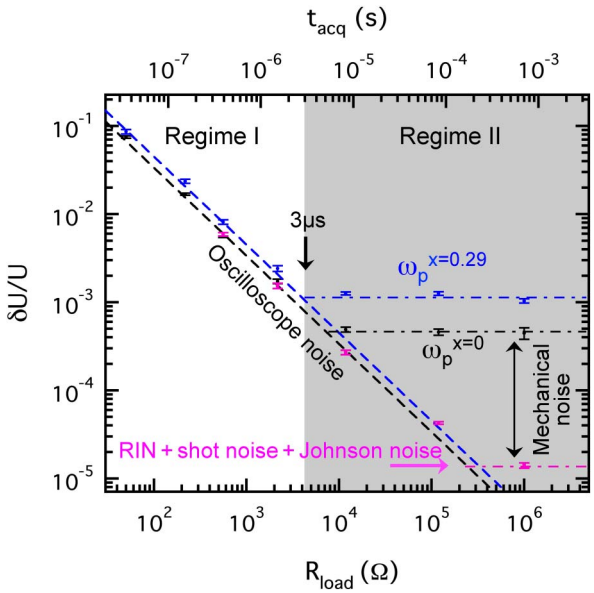

Fig. 2. Noise-to-signal ratio $\delta U/U$ of the photovoltage U induced by the radiated field from the PhC cavity versus the load resistance R_{load} of the photodetector, and the corresponding acquisition sampling time t_{acq} for pump frequency detunings of $x = 0$ (dark points) and $x = 0.29$ (blue points). The error bars correspond to the standard deviation of ten repeated measurements. The black and blue dashed lines correspond to the noise limit imposed by the oscilloscope for $x = 0$ and $x = 0.29$, respectively. The collected powers measured at resonance with $R_{load} = 1$ MΩ for $x = 0$ and $x = 0.29$ are 8 μW and 6 μW, respectively. Purple data points: noise-to-signal ratio without any PhC cavity between the laser source and the photodetector for the same collected power, as in the case of $x = 0$. The gray area corresponds to a regime limited by the fundamental thermo-optic noise.

is plotted versus the load resistance and the acquisition sampling time for a pump frequency in resonance with the frequency of the cavity ω_0 ($x = 0$), see black data points with error bars, and for a detuning $x = 0.29$, see blue data points. The values of $\delta U/U$ are determined from temporal signal traces similar to the ones in Fig. 1(b). For a load resistance of 1 MΩ, the average photovoltage U amounts to 8 V for $x = 0$ and 6 V for $x = 0.29$. Considering that the responsivity of the photodetector is $G \sim 1$ A/W, the collected power at resonance is 8 μW. In both cases, two regimes take place: for $t_{acq} < 3$ μs, $\delta U/U$ decreases linearly (regime I), whereas for $t_{acq} > 3$ μs, it is independent of the acquisition sampling time (regime II). As confirmed by the black and blue dashed lines, regime I can be explained by taking into account the standard deviation $\delta U_{osc} = 30$ μV of the electronic noise of the fast oscilloscope. In this regime, the noise-to-signal ratio drops by increasing the value of the collected signal. In regime II, which is indicated by the gray area, the noise at resonance ($x = 0$) is larger than the expected contribution from the sum of the RIN of the laser source, the shot noise, and the Johnson noise. The purple data points correspond to this sum of noise contributions. We attribute the difference between the noise floor level measured at $x = 0$ (black data points) and the intensity noise floor of the laser source to the intensity instability induced by the mechanical vibrations of the setup.

3. CAVITY SPECTRAL NOISE

The noise-to-signal ratio can be separated into two contributions as $(\delta U/U)^2 = (\delta U/U|_{\delta\omega})^2 + (\delta U/U|_I)^2$. The first contribution is associated to fluctuations of the scattered intensity δI^{scat} that are triggered by a frequency noise $\delta\omega$, whereas $\delta U/U|_I$ takes into account all other sources of noise. The intensity variation δI^{scatt} is related to the frequency shift of the perturbed cavity via the envelope of the cavity mode spectrum. This envelope is well modeled with a Lorentzian profile (see Supplement 1),

$$S(\omega_0, \omega_p) = \frac{1/4Q^2}{((\omega_p - \omega_0)/\omega_0)^2 + 1/4Q^2}\frac{I^{scat}}{I^{in}}, \quad (1)$$

where I^{in} is the incident power in the access waveguide coupled to the cavity. The relative intensity fluctuation is given by $\delta I^{scat}/I^{in} = S(\omega_0 + \delta\omega, \omega_p) - S(\omega_0, \omega_p)$, and depends on the detuning x between the frequencies of the pump and of the cavity resonance. It follows that

$$\delta U/U|_{\delta\omega} = -1 + \frac{1 + 4x^2}{1 + 4\left(\frac{x - \delta\omega/\Delta\omega}{1 + \delta\omega/\Delta\omega/Q}\right)^2}. \quad (2)$$

Measuring the noise-to-signal ratio at $x = 0$ and $x = 0.29$ allows us to retrieve the experimental values of the relative frequency noise $\delta\omega/\Delta\omega = 5.8 \pm 0.5 \times 10^{-4}$, and of the contribution $\delta U/U|_I = 4.5 \pm 0.5 \times 10^{-4}$. The laser source has a spectral linewidth of 200 kHz. It corresponds to a relative frequency noise $\delta\omega/\Delta\omega|_{laser} = 4 \times 10^{-6}$, which is 2 orders of magnitude smaller than the retrieved experimental value. Consequently, we attribute the current spectral noise to the thermorefractive noise, which is also supported by Fig. 3.

In Fig. 3, we compare the ratio $\delta U/U$ for three different L3 cavities, including the one of $Q = 3800$ studied in Fig. 1, and for $x = 0$ and $x = 0.29$. One of these cavities has a Q factor of 2200, and differs from the previous one by its separation of three lines of holes between the W1 access waveguide and the cavity defect. This cavity operates almost in the optimal coupling condition based on simulation of the intrinsic Q factor of the cavity. For the third cavity, whose Q factor amounts to 16,800 and whose coupling is identical to the one of the cavity of $Q = 3800$, the first three holes located on both sides of the line defect have been slightly laterally shifted away from the core by a length of (0.2 a, 0.025 a, 0.2 a), as initially proposed in [12,13].

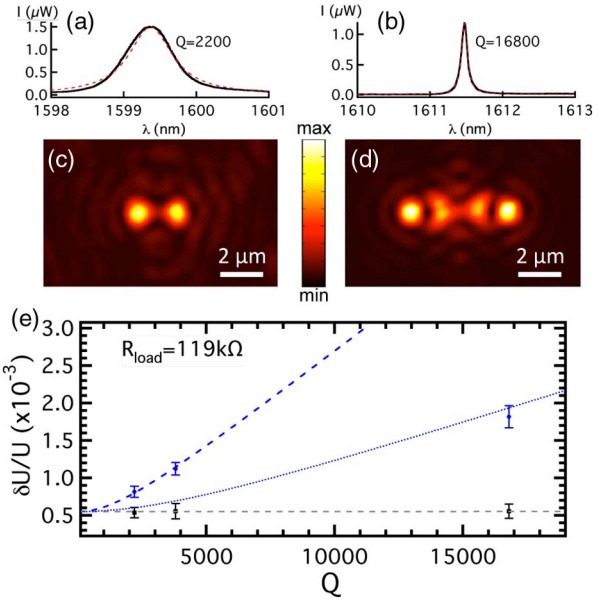

Fig. 3. (a) and (b) Optical spectra of L3 PhC cavities with $Q = 2200$ and $Q = 16800$, respectively. The red dotted lines are Lorentzian fits. (c) and (d) Near-infrared optical images of the resonant field radiated from the $Q = 2200$ and $Q = 16800$ PhC cavities, respectively. (e) Noise-to-signal ratio $\delta U/U$ of the photo voltage U versus the quality factor for $x = 0$ (black dashed line) and $x = 0.29$ (blue dashed line) with a load resistance of $R_{load} = 119$ kΩ. Black and blue dashed lines are expected variations with the effective mode volume of the $Q = 3800$ cavity. The blue dotted line is the expected variation with the effective mode volume of the $Q = 16800$ cavity. The collected power at $x = 0$ is 0.17 μW.

No variation of the ratio $\delta U/U$ versus the Q factor is observed for $x = 0$. On the other hand, the case $x = 0.29$ exhibits an increasing variation of $\delta U/U$ versus the Q factor. Both trends are expected for a constant and sufficiently small frequency noise. As regards the cavity of $Q = 16{,}800$, its $\delta U/U$ value is nevertheless 2.4 times smaller than the expected value from Eq. (2) (see blue dashed line in Fig. 3). The origin of this departure lies in the larger mode volume of this cavity as explained below. The difference in mode volume is revealed by a larger spatial distribution of the intensity of the cavity mode in Fig. 3(d) compared to the one of the cavities of lower Q in Fig. 3(c). Note that the impact of the volume on $\delta U/U$ definitely excludes any major contribution of the laser frequency ω_p noise.

4. FUNDAMENTAL THERMOREFRACTIVE NOISE

Any medium of density ρ in thermal equilibrium at a temperature T is subject to fundamental thermal fluctuations [14]. The variance of these fluctuations in a local volume V of the medium is given by $\delta T^2 = \frac{k_B T^2}{(\rho V) C_V}$, where k_B is the Boltzmann constant and C_V the heat capacity at constant volume. The thermal

fluctuations δT within the cavity mode volume induce a frequency noise on the resonant frequency ω_0 of the cavity. It results from the perturbation of the dielectric constant of the medium that depends on the temperature via the optical index n and the thermo-optic coefficient $\frac{\partial n}{\partial T}$ [15]. Based on a perturbation approach, the relative frequency noise is given by

$$\delta\omega/\Delta\omega = Q\delta\omega/\omega_0 = \frac{Q}{n}\left(\frac{\partial n}{\partial T}\right)\sqrt{\frac{k_B T^2}{(\rho V_{\text{ovl}})C_V}}, \quad (3)$$

where V_{ovl} is an interaction overlap volume between the cavity mode and the thermal fluctuations [16]. For a cavity mode of electric field distribution E, the volumes V_{eff} and V_{ovl} are functionals of $|E|^2$ and $|E|^4$, repectively. Assuming a Gaussian distribution of the cavity field intensity, $V_{\text{ovl}} = 2\sqrt{2}V_{\text{eff}}$. Based on the experimental value of the relative frequency noise $\delta\omega/\Delta\omega = 5.8 \times 10^{-4}$, the thermo-optic coefficient of the silicon $(\frac{\partial n}{\partial T}) = 1.8 \times 10^{-4}$ [17] and the effective optical index of the silicon slab waveguide $n = 2.74$ [18], we obtain $V_{\text{ovl}} = 0.13\ \mu\text{m}^3$, which is of the same order of magnitude as $2\sqrt{2}V_{\text{eff}} = 0.17\ \mu\text{m}^3$.

Achieving the fundamental thermodynamic noise level with passive optical systems based on large effective mode volumes, such as in optical fiber sensors [19–22], is challenging in general, as it requires ultrastable laser sources. With PhC cavities, the effective mode volume is small enough to boost the thermodynamic noise level beyond the noise level of standard diode-laser sources. In particular, advanced lock-in techniques [23] are superfluous with these cavities.

From the experimental near-field pattern of the cavity modes [24], we have estimated the effective mode volume and the interaction overlap volume of the $Q = 16{,}800$ cavity mode to be 2.1 and 5.2 times larger than the corresponding ones of the standard L3 cavity, respectively. The factor 2.1 is in agreement with the far-field real-space images of the intensity distribution of the cavity modes in Figs. 3(a) and 3(b). Considering that the frequency noise varies with the square root of the overlap volume $\sqrt{V_{\text{ovl}}}$, the factor $\sqrt{5.2} \simeq 2.3$ explains the drop of $\delta U/U$ by a factor 2.4 for the cavity of $Q = 16{,}800$. The extended mode volume of this cavity, whose theoretical intrinsic Q factor amounts to 65,000 for the current slab thickness, is attributed to a strong coupling with the W1 waveguide.

5. ULTIMATE DETECTION LIMIT

The measured voltage noise $\delta U/U$ allows us to define an ultimate minimal relative frequency shift $\delta\omega/\Delta\omega|_{\text{min}}$. Any frequency shift that is induced by a nanoparticle located in the surrounding of the cavity mode can be distinguished from the noise with a probability larger than 68%, i.e., "one-sigma" confidence interval, if it is larger than one time $\delta\omega/\Delta\omega|_{\text{min}}$. The minimal frequency noise that takes into account not only the intrinsic frequency noise, but also any extrinsic intensity noise of the signal, is given by

$$\left.\frac{\delta\omega}{\Delta\omega}\right|_{\text{min}} = -Q + \frac{x + Q}{1 + (2Q)^{-1}\sqrt{[(4x^2+1)^{-1} + \delta U/U]^{-1} - 1}}. \quad (4)$$

It depends on the detuning x, and for a fixed $\delta U < 0.01U$ reaches a minimal value for $x \simeq 0.29$. This figure of merit is plotted in Fig. 4(a) versus the acquisition sampling time for $x = 0.29$ and for the three cavities [25]. The three cavities are excited with

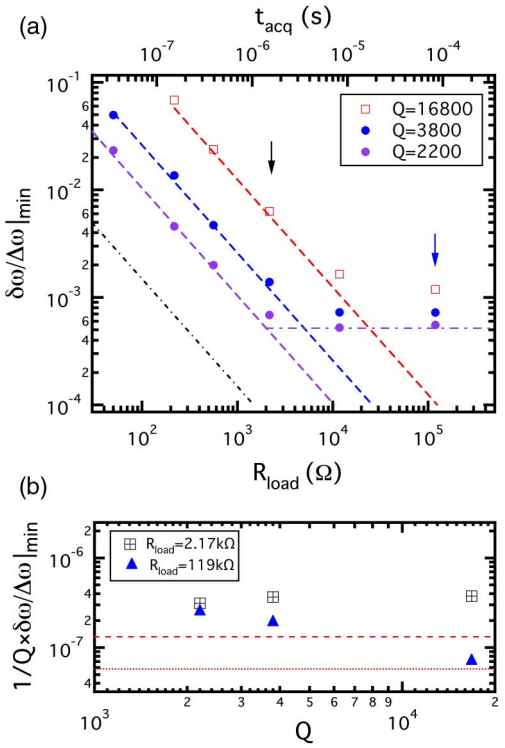

Fig. 4. (a) Square and circle symbols are the minimum relative frequency shift that can be detected versus the load resistance R_{load}, and the corresponding acquisition time t_{acq} for three different quality factors Q with the same input power and the same frequency detuning $x = 0.29$. The purple, blue, and red dashed lines are oscilloscope noise limits for the powers of 15, 6, and 1.25 μW that are collected with $R_{\text{load}} = 1\ \text{M}\Omega$ for each cavity, respectively. Dark dot-dashed line is the oscilloscope noise for an optimal light collection. The purple dot-dashed line pinpoints the saturation level due to the thermal and mechanical noise for $Q = 2200$. (b) Minimum relative frequency shift normalized to the quality factor for two load resistances pinpointed by the black and blue arrows in (a). The red dashed line and dotted line are the fundamental thermal noise limits associated with a fundamental mode volume of $V_{\text{eff}} = 0.060\ \mu\text{m}^3$ (i.e., for $Q = 2200$ and $Q = 3800$) and $V_{\text{eff}} = 0.126\ \mu\text{m}^3$ (i.e., for $Q = 16800$), respectively.

the same power of 15.6 mW at the input of the photonic chip. In term of frequency noise, the cavity with the lowest Q factor outperforms the other ones in the regime that is governed by the oscilloscope noise. It results from a better light coupling. A figure of merit of 1/45 is achievable with an acquisition sampling time of 30 ns. When $t_{\text{acq}} > 2\ \mu\text{s}$, the figure of merit reaches 1/2000, which is 1 order of magnitude larger that the values reported in [26].

Note that the signal inside the numerical aperture of the collection path of the setup is attenuated by a factor of 7 until the photodetector, mainly due to the transmission through the high-NA microscope objective and a 50/50 beam splitter. The dot-dashed line corresponds to the expected oscilloscope noise limit in the case of the cavity of $Q = 2200$, but without this extrinsic attenuation factor that can be cancelled by integrating the photodetector directly on chip. In this case, a figure of merit of 1/2000 is reachable with an acquisition sampling time of 100 ns.

Based on the knowledge of the figure of merit, the minimal nanoparticle volume $V_{\text{part}}^{\text{min}}$ that is detectable can be estimated from a first-order perturbation approach by considering the

photonic system as a closed system. The relative frequency shift induced by the modification $\delta\epsilon$ of the refractive index map due to the presence of the nanoparticle at a location where the cavity field intensity is $\|E_{\text{part}}\|^2$ can be approximated by (see Supplement 1)

$$\left.\frac{\delta\omega}{\omega_0}\right|_{\text{pert}} = -\frac{1}{2}\frac{\delta\epsilon}{\epsilon_c+\delta\epsilon}\frac{V_{\text{part}}}{V_{\text{eff}}}\frac{\|E_{\text{part}}\|^2}{\|E_{\max}\|^2}, \tag{5}$$

with ϵ_c the unperturbed dielectric constant at the position of the dielectric perturbation, namely the nanoparticle. Eq. (5) is a good approximation for high-Q cavities, i.e., when any energy dissipation is neglected. As discussed in [27] and references therein, in the case of strong radiation leakage or absorption, the standard effective mode volume can be replaced by a generalized mode th volume that takes into account the complex nature of the wave vector of the mode. The current approach that is based on a first-order perturbation of a Hermitian operator and the one developed in [27] are compared in Supplement 1. In the following, we adopt the closed system approximation in view of the high quality factor of the current cavities. As a result, the minimal particle volume can be expressed as

$$V_{\text{part}}^{\min} = 2\frac{\epsilon_c+\delta\epsilon}{\delta\epsilon}\frac{\|E_{\max}\|^2}{\|E_{\text{part}}\|^2}\frac{V_{\text{eff}}}{Q}\left.\frac{\delta\omega}{\Delta\omega}\right|_{\min}. \tag{6}$$

It follows that $V_{\text{part}}^{\min}/V_{\text{eff}} \propto \delta\omega/\Delta\omega|_{\min}/Q$, which is plotted in Fig. 4(b) versus the Q factor for the three cavities, and for the two different regimes pinpointed by the blue ($R_{\text{load}} = 119$ kΩ) and black arrows ($R_{\text{load}} = 2.17$ kΩ) in Fig. 4(a). In the regime limited by the electronic noise (see black squares with cross) the cavity of $Q = 2200$ allows detection of the smallest particle, whereas in the regime limited by the thermal noise (blue triangles), increasing the quality factor improves the detection limit. This improvement comes from a relative drop of the noise contribution due to extrinsic intensity noise ($\delta U/U|_I$). As revealed by the red dashed line that corresponds to the previously determined intrinsic thermal noise limit, $V_{\text{part}}^{\min}/V_{\text{eff}}$ is independent of Q, and equal to a constant of 1.3×10^{-7} for the mode volume of the cavities of quality factor 2200 and 3800. This constant drops to 5.8×10^{-8} for the cavity of quality factor 16,800 due to a larger mode volume (see red dotted line). Although the thermal frequency noise $\delta\omega/\Delta\omega|_T$ is lower for larger effective mode volume, it does not mean that a larger V_{eff} leads to a better detection limit for nanoparticle sensing, as indicated in Fig. 5.

In Fig. 5, the ultimate relative frequency shift $\delta\omega/\Delta\omega|_T$ [see Eq. (3)] that corresponds to the fundamental thermal noise limit has been normalized to Q/V_{eff} and plotted versus the effective mode volume. $V_{\text{eff}}/Q\times\delta\omega/\Delta\omega|_T$, which is proportional to the ultimate minimal detectable nanoparticle volume, follows a square root variation when the fundamental thermal limit is reached. The square root variation of the thermal frequency noise, i.e., its sublinear variation, versus the effective mode volume implies that V_{eff} still needs to be minimized to improve the detection limit in the case of single nanoparticle sensing. In contrast, the quality factor has no impact on the detection limit when the fundamental thermal limit has been reached [see Fig. 4(b)].

Based on our experimental determination of the minimal relative frequency shift $\delta\omega/\Delta\omega|_{\min}$, we can estimate the minimal size of a colloidal nanoparticle that can be detected for a given acquisition speed. We consider the case of a single silica nanoparticle in air and of a biological nanoparticle in water. In the case of a single silica nanoparticle ($n_{SiO_2} = 1.44$) located in the air at a position of 10 nm from the surface of the silicon membrane, and at the smallest distance from the maximum value of the cavity field intensity, which corresponds to $\frac{|E_{\max}|^2}{|E_{\text{part}}|^2} \simeq 1.76$, the minimum detectable equivalent spherical radius within a 1-sigma confidence interval is $r_{SiO_2}^{\min} = 5.5$ nm for the cavity of $Q = 3800$ and $t_{\text{acq}} = 10$ μs, and $r_{SiO_2}^{\min} = 4.8$ nm when the fundamental thermal limit is reached [see red dashed line in Fig. 4(b)]. It rises to 7.0 nm for a 3-sigma confidence interval. With $t_{\text{acq}} = 30$ ns, our current experimental limit provides $r_{SiO_2}^{\min} =$ 21.0 nm/30.3 nm for the 1-sigma/3-sigma confidence interval. By optimizing the light collection [see black dot-dashed line in Fig. 4(a)], a detection limit of $r_{SiO_2}^{\min} = 10$ nm with $t_{\text{acq}} =$ 30 ns is achievable. As regards a biological nanoparticle in water ($n_{\text{water}} \sim 1.3$), e.g., an extracellular vesicle such as an exosome [28,29] ($n \sim 1.5$), the optical index contrast is ~0.2, which leads to $r_{\text{bio}}^{\min} \simeq 5.4$ nm/7.8 nm for the 1-sigma/3-sigma confidence interval and $t_{\text{acq}} = 10$ μs. Such values rely on the assumption that water does not induce extra fluctuations. For $t_{\text{acq}} = 30$ ns, the minimum equivalent spherical radius drops to $r_{\text{bio}}^{\min} \simeq$ 23.3 nm/33.7 nm for the 1-sigma/3-sigma confidence interval.

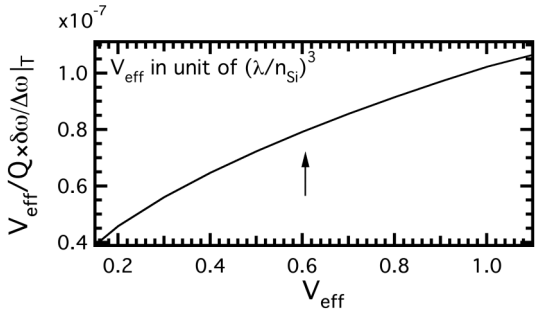

Fig. 5. Relative frequency shift $\delta\omega/\Delta\omega|_T$ induced by the fundamental thermal noise normalized to Q/V_{eff} versus the effective cavity mode volume V_{eff}. This quantity is proportional to the minimal nanoparticle volume that the sensor can detect when the fundamental thermal noise limit is reached. The arrow pinpoints the value for the standard L3 PhC cavity. V_{eff} is normalized to $(\lambda/n_{\text{Si}})^3$ where n_{Si} is the index of the silicon material and the wavelength $\lambda = 1.6$ μm.

6. CONCLUSION

To conclude, we have quantified the intrinsic detection limit of integrated PhC cavities and identified the main limiting factors. Importantly, for an effective mode volume of 0.06 μm^3 we have reached a value $\delta\omega/\Delta\omega|_{\min} = 1.9\times10^{-7}\times Q$, which is very close to the ultimate limit $\delta\omega/\Delta\omega|_T = 1.3\times10^{-7}\times Q$ that is imposed by the fundamental thermodynamic fluctuations at room temperature. We have well posed the problem of the detection limit by considering the acquisition sampling time, and in a similar way to [10] we propose $V_{\text{eff}}/Q\times\delta\omega/\Delta\omega|_{\min}\times t_{\text{acq}}$ as a relevant figure of merit to compare the performance of optical cavity sensors. When dissipation effects are not negligible, for instance, for the case of plasmonic resonances, V_{eff} can be replaced by a generalized mode volume as introduced in [27].

The fundamental noise limit is currently reached for an acquisition sampling time $t_{\text{acq}} \geq 3$ μs. Improving the amount of light collected out of the cavity is necessary to further push the minimal acquisition sampling time. The current study makes it possible to

answer the question: what is the trade-off between the acquisition speed and the detection limit to track a nanoparticle in real time with a resonant cavity field? In particular, our study shows that a single PhC cavity enables us to monitor up to 33 million particles per second with a particle size down to 34 nm with the currently achieved experimental conditions, and down to 10 nm by optimizing the light collection. From another point of view, knowing the value of the ultimate intrinsic noise level allows tracking of the origin of any extrinsic fluctuations that are larger than the thermal fluctuations. For instance, fundamental fluctuations in liquid can, in principle, be investigated at the nanoscale, and with a temporal resolution of few nanoseconds by using a PhC cavity. In this context we envision that our methodology will be of high interest for identifying the ultimate performances of optical biosensors and airborne nanoparticle sensors.

Moreover, as the Brownian motion of single nanoparticles is dependent on the morphology of the nanoparticle, their tracking via the intensity fluctuations of a cavity mode has the potential for an unprecedentedly accurate and noninvasive characterization of colloidal solutions. Our approach can circumvent limitations intrinsic to fluorescence correlation spectroscopy [30]. In general terms, our experimental results suggest that implementing an integrated dynamic light scattering technique [31] is feasible with PhC cavities, which can trigger a major impact in the field of medical diagnostics and for the analysis of hazardous aerosols.

7. METHODS

The PhC cavities are optically excited with a tunable laser source from Santec (TSL-510 type C). A 1.2 GHz InGaAs photodiode from Thorlabs (DET01CFC) detects the scattered intensity and the corresponding photovoltage is recorded with a 1 GHz oscilloscope from Agilent Technologies (DS06104A).

The light coupling into the photonic chip is ensured by a lensed fiber mounted on a nanopositioning stage. This mechanical stage, and another one that enables the light collection through the microscope objective, represent the main sources of mechanical vibrational noise.

The total number of data points N_p for each of the recorded time traces, and the time window Δt that have been used to determine U are given in Table 1. The standard deviation that is defined in a classical way as $\delta U = \{\frac{1}{N_p-1}\sum_{i=1}^{N_p}(U(t_i) - \langle U\rangle)^2\}^{1/2}$ depends on the total number of data points N_p for each of the recorded time traces. $U(t_i)$ is the photovoltage signal at a time t_i and $\langle U\rangle$ is the average value of the photovoltage over the time window Δt. The acquisition sampling time t_{acq} is defined by the constant interval $t_{i+1} - t_i$. The time window and the number of points, and consequently $t_{\mathrm{acq}} = \Delta t/N_p$, have been chosen to be in line with the response time of the detection system.

Table 1. Settings to Determine the Standard Deviation δU

Load Resistance	N_p	Δt
50 Ω	250,000	50 ms
218 Ω	250,000	50 ms
560 Ω	250,000	0.1 s
2.17 kΩ	250,000	0.5 s
11.8 kΩ	50,000	0.5 s
119 kΩ	50,000	5 s
1 MΩ	500	0.5 s

Acknowledgment. The authors acknowledge the support of the MRP multidisciplinary research platform initiative at Ghent University through NB-Photonics, and thank R. Baets for critical comments on the paper.

See Supplement 1 for supporting content.

REFERENCES AND NOTES

1. K. J. Vahala, "Optical microcavities," Nature **424**, 839–846 (2003).
2. M. G. Scullion, T. F. Krauss, and A. Di Falco, "Slotted photonic crystal sensors," Sensors **13**, 3675–3710 (2013).
3. F. Vollmer, S. Arnold, and D. Keng, "Single virus detection from the reactive shift of a whispering-gallery mode," Proc. Natl. Acad. Sci. USA **105**, 20701–20704 (2008).
4. S. Rosenblum, Y. Lovsky, L. Arazi, F. Vollmer, and B. Dayan, "Cavity ring-up spectroscopy for ultrafast sensing with optical microresonators," Nat. Commun. **6**, 6788 (2015).
5. M. Tardif, J.-B. Jager, P. R. Marcoux, K. Uchiyamada, E. Picard, E. Hadji, and D. Peyrade, "Single-cell bacterium identification with a SOI optical microcavity," Appl. Phys. Lett. **109**, 133510 (2016).
6. F. Priolo, T. Gregorkiewicz, M. Galli, and T. F. Krauss, "Silicon nanostructures for photonics and photovoltaics," Nat. Nanotechnol. **9**, 19–32 (2014).
7. D. Keng, S. McAnanama, I. Teraoka, and S. Arnold, "Resonance fluctuations of a whispering gallery mode biosensor by particles undergoing Brownian motion," Appl. Phys. Lett. **91**, 103902 (2007).
8. From the local intensity $|E|^2$ of the cavity mode and the dielectric map ϵ of the photonic structure, the effective volume can be defined as $V_{\mathrm{eff}} = \int \epsilon|E|^2 dV/\max\{\epsilon|E|^2\}$, where the *max* function takes the maximum value over the entire space. The numerical value $V_{\mathrm{eff}} = 0.06\ \mu\mathrm{m}^3$ has been determined with a finite difference time-domain method.
9. X. Zhou, L. Zhang, and W. Pang, "Performance and noise analysis of optical microresonator-based biochemical sensors using intensity detection," Opt. Express **24**, 18197–18208 (2016).
10. J. Hu, X. Sun, A. Agarwal, and L. C. Kimerling, "Design guidelines for optical resonator biochemical sensors," J. Opt. Soc. Am. B **26**, 1032–1041 (2009).
11. Note that the current definition of the acquisition time is much more restrictive than the conventional definition of the rise time, which amounts to 6 μs for a load resistance of 1 MΩ with the current photodetector bandwidth of 1.2 GHz at $R_{\mathrm{load}} = 50\ \Omega$.
12. Y. Akahane, T. Asano, B.-S. Song, and S. Noda, "High-Q photonic nanocavity in a two-dimensional photonic crystal," Nature **425**, 944–947 (2003).
13. Y. Akahane, T. Asano, B.-S. Song, and S. Noda, "Fine-tuned high-Q photonic-crystal nanocavity," Opt. Express **13**, 1202–1214 (2005).
14. L. D. Landau and E. M. Lifshitz, *Statistical Physics, Part 1*, 3rd ed. (Pergamon, 1980), § 114.
15. In view of the value of the thermal expansion coefficient of the silicon, the impact of the density fluctuations can be neglected here.
16. M. L. Gorodetsky and I. S. Grudinin, "Fundamental thermal fluctuations in microspheres," J. Opt. Soc. Am. B **21**, 697–705 (2004).
17. J. Komma, C. Schwarz, G. Hofmann, D. Heinert, and R. Nawrodta, "Thermo-optic coefficient of silicon at 1550 nm and cryogenic temperatures," Appl. Phys. Lett. **101**, 041905 (2012).
18. As a first-order approximation, we assume that mode is located within a homogeneous medium whose index equals the effective index of the 215 nm thick silicon slab waveguide. The optical index of the silicon is 3.45.
19. G. Gagliardi, M. Salza, S. Avino, P. Ferraro, and P. De Natale, "Probing the ultimate limit of fiber-optic strain sensing," Science **330**, 1081–1084 (2010).
20. G. A. Cranch and S. Foster, "Comment on probing the ultimate limit of fiber-optic strain sensing," Science **335**, 286 (2012).
21. G. Gagliardi, M. Salza, S. Avino, P. Ferraro, and P. De Natale, "Response to comment on probing the ultimate limit of fiber-optic strain sensing," Science **335**, 286 (2012).
22. J. Dong, J. Huang, T. Li, and L. Liu, "Observation of fundamental thermal noise in optical fibers down to infrasonic frequencies," Appl. Phys. Lett. **108**, 021108 (2016).
23. J. Knittel, J. D. Swaim, D. L. McAuslan, G. A. Brawley, and W. P. Bowen, "Back-scatter based whispering gallery mode sensing," Sci. Rep. **3**, 2974 (2013).

24. We have implemented a scanning near-field technique making use of silica nanotips to map the cavity near field, which will be discussed elsewhere.
25. Note that even if the total quality factor appears as a parameter in Eq. (4), it has no impact on $\delta\omega/\Delta\omega|_{\min}$, as expected from the normalization by $\Delta\omega$, which confers to this quantity a figure of merit character.
26. F. Vollmer and L. Yang, "Label-free detection with high-Q microcavities: a review of biosensing mechanisms for integrated devices," Nanophotonics **1**, 267–291 (2012).
27. J. Yang, H. Giessen, and P. Lalanne, "Simple analytical expression for the peak-frequency shifts of plasmonic resonances for sensing," Nano Lett. **15**, 3439–3444 (2015).
28. S. El Andaloussi, I. Mäger, X. O. Breakefield, and M. J. A. Wood, "Extracellular vesicles: biology and emerging therapeutic opportunities," Nat. Rev. Drug Discovery **12**, 347–357 (2013).
29. C. Théry, M. Ostrowski, and E. Segura, "Membrane vesicles as conveyors of immune responses," Nat. Rev. Immunol. **9**, 581–593 (2009).
30. M. Eigen and M. Rigler, "Sorting single molecules: application to diagnostics and evolutionary biotechnology," Proc. Natl. Acad. Sci. USA **91**, 5740–5747 (1994).
31. B. J. Berne and R. Pecora, *Dynamic Light Scattering: With Applications to Chemistry, Biology, and Physics* (Wiley, 1976).